

# 1 The OMZ and nutrients features as a signature of inter-annual and 2 low-frequency variability off the Peruvian upwelling system

3  
4 Michelle I. Graco<sup>1</sup>, Sara Purca<sup>1</sup>, Boris Dewitte<sup>2,3,4</sup>, Carmen G. Castro<sup>5</sup>, Octavio Morón<sup>1</sup>, Jesús Ledesma<sup>1</sup>,  
5 Georgina Flores<sup>1</sup>, Dimitri Gutiérrez<sup>1</sup>

6 <sup>1</sup>Dirección General de Investigaciones Oceanográficas y cambio Climático. Instituto del Mar del Perú (IMARPE), P.O. Box  
7 22, Callao, Perú.

8 <sup>2</sup>Laboratoire d'Etudes en Géophysique et Océanographie Spatiale (LEGOS)/IRD, Toulouse, France

9 <sup>3</sup>Universidad Católica del Norte, Facultad de Ciencias del Mar, Coquimbo, Chile

10 <sup>4</sup>Centro de Estudios Avanzado en Zonas Áridas (CEAZA), Coquimbo, Chile

11 <sup>5</sup>CSIC, Instituto de Investigaciones Marinas, Eduardo Cabello 6, 36208 Vigo, Spain.

12  
13 *Correspondence to:* Michelle I. Graco (mgraco@imarpe.gob.pe)

14 **Abstract.** Over the last decades, the Humboldt Current Upwelling Ecosystem and particularly the Northern component off  
15 Peru, has drawn the interest of the scientific community because of its unique characteristics: it is the upwelling system with  
16 the biggest catch productivity, despite the fact it is embedded in a shallow and intense Oxygen Minimum Zone (OMZ). It is  
17 also an area of intense nitrogen loss and anammox activity and experiences a large inter-annual variability associated with the  
18 equatorial remote forcing. In this context, we examined the oceanographic and biogeochemical variability associated with the  
19 OMZ off central Peru, from a monthly time series (1996–2011) recorded off Callao (12°02'S, 20 nm). The data reveals a rich  
20 spectrum of variability of the OMZ that includes frequencies ranging from seasonal to inter-annual scales. Due to the efficient  
21 oceanic teleconnection off Peru, the observed variability is interpreted in the light of an estimate of the equatorial Kelvin wave  
22 contribution to sea level anomalies considering peculiarities of its vertical structure (i.e. first two baroclinic modes). The span  
23 of the data set allows contrasting two OMZ regimes. The “strong” regime associated with the strong 1997–1998 Equatorial  
24 Pacific El Niño, during which the OMZ adjusted to Kelvin wave-induced downwelling conditions that switched off the  
25 upwelling and drastically reduced nutrients availability. The “weak” regime corresponding to the post-2000 period associated  
26 to the occurrence of moderate Central Pacific El Niño events and enhanced equatorial Kelvin wave activity, in which mean  
27 upwelling conditions are maintained. It is shown that the characteristics of the coupling between physics and biogeochemistry  
28 is distinct between the two regimes, with the “weak” regime being associated to a larger explained variance in biogeochemical  
29 properties not related to the ENSO oceanic teleconnection. The data also reveals a long-term trend from 1999 corresponding  
30 to a deepening of the oxygen deficient waters and a warming. Implications of our results for understanding the OMZ dynamics  
31 off Peru are discussed.

## 32 1 Introduction

33  
34 The upwelling region off Peru hosts a complex biogeochemical system that is unique for at least two reasons. First, it is  
35 embedded into the permanent, intense and shallow Oxygen Minimum Zone (OMZ) of the Eastern Tropical South Pacific  
36 (Gutiérrez et al., 2008). Second, it exhibits a significant variability at different time scales, particularly at inter-annual scale  
37 associated with the Equatorial Kelvin waves and the El Niño-Southern Oscillation, ENSO (Chavez et al., 2008).

38 The OMZ is generated by the combination of high oxygen demand during organic matter remineralization and the sluggish  
39 ventilation in the region (Wyrski, 1962; Helly and Levin, 2004). It is wide in the vertical extension (~ 500 m), intense (< 22.5  
40  $\mu\text{mol kg}^{-1}$ ), and at some latitudes the upper boundary could be very shallow (25-50 m) intersecting the euphotic zone and

41 impinging the continental shelf (Morales et al., 1999; Schneider et al., 2006; Fuenzalida et al., 2009; Paulmier and Ruiz, 2009;  
42 Ulloa and Pantoja, 2009). The OMZ off Peru is associated with the presence of nutrient-rich Equatorial Subsurface Water  
43 (ESSW) transported poleward by the Peru-Chile Undercurrent (PCU) (Strub et al., 1998; Fuenzalida et al., 2009; Silva et al.,  
44 2009) and the transport of low-oxygenated waters by the narrow primary and secondary Southern Subsurface Countercurrents  
45 near 4°S and 7°S respectively also known as Tsuchida jets (Furue et al., 2007; Montes et al., 2010). Recent modeling studies  
46 also highlight the important role of sub to mesoscale dynamics in constraining the upper OMZ meridional boundaries  
47 (Bettencourt et al., 2015; Vergara et al., 2016).

48 The OMZ variability in terms of distribution and intensity has a direct impact on the biogeochemical processes of the  
49 northern region of the Humboldt upwelling system, because oxygen: 1) is a key factor in biogeochemical cycles, particularly  
50 in the carbon (Friederich et al., 2008) and nitrogen processes (e.g. Kock et al., 2016; Hammersley et al., 2007; Lam and  
51 Kuypers, 2011; Dale et al., 2017), 2) its consumption determines high nitrogen loss and in consequence low N:P ratio of  
52 upwelled waters, below the classical Redfield ratio of 16, with a strong impact on the primary and secondary production (Franz  
53 et al., 2012) and 3) is a control factor in the distribution of organisms (e.g. Bertrand et al., 2010; Criales-Hernández et al.,  
54 2006; Ekau et al., 2010; Gutiérrez et al., 2008, Levin et al, 2002). The position, strength, and thickness of the Eastern South  
55 Pacific OMZ can be greatly modified by local and/or remote forcing (e.g. inter-annual time scales, Morales et al., 1999;  
56 Gutiérrez et al., 2008). During ENSO episodes, equatorial fluctuations in sea level and currents propagate along the Peruvian  
57 coast, which behaves as an extension of the equatorial waves guide (Clarke and van Gorder, 1994). Strong El Niño (EN)  
58 events, like the 1997-1998 Eastern Pacific El Niño, affect the circulation and water masses distribution causing the deepening  
59 of the OMZ and the occurrence of large oxygenation events in the water column and over the sediments along the Chilean and  
60 Peruvian coast (Morales et al., 1999; Sánchez et al., 1999; Gutiérrez et al., 2008). In fact, Helly and Levin (2004) reported  
61 that, during the 1997-1998 El Niño, about 61% of the OMZ volume off Peru and northern Chile was reduced.

62 While most studies on the inter-annual impact have focused on the 1997-1998 El Niño, recent studies indicate that  
63 the characteristics of the inter-annual variability have changed in the last decades. In fact, since the 90s a higher frequency of  
64 the so-called Central Pacific (or Modoki) El Niño events occurs (Yeh et al., 2009; Lee and McPhaden, 2010; Takahashi et al.,  
65 2011). This type of El Niño event does not undergo a significant warming of Sea Surface Temperature (SST) along the coast  
66 of Peru conversely to Eastern Pacific El Niño events (Ashok et al., 2007; Dewitte et al, 2012). On the other hand, Central  
67 Pacific El Niño events are associated with strong activity of Intra-seasonal Equatorial Kelvin Waves (IEKW) (Mosquera et al.,  
68 2014) that can lead to thermocline depth fluctuations along the coast of Peru through the propagation of coastally trapped  
69 Kelvin waves (cTKW) (Clarke, 1983; Dewitte et al., 2011; Illig et al., 2014).

70 The study of the relationship between ENSO and the OMZ therefore, would require taking into account the different  
71 time scales of variability along the equator, from intra-seasonal to inter-annual. Most existing studies have documented the  
72 physical properties (Morón O., 1991; 2000) and chemical properties of the waters along the coast of Peru in relation with the  
73 inter-annual equatorial variability (Calienes and Guillén, 1981; Guillén and Izaguirre de Rondán, 1973; Guillén et al., 1989;  
74 Ledesma et al., 2011) disregarding the higher-frequency time scales and the diversity of ENSO (Capotondi et al., 2015). Here,  
75 we analyze a unique long-term time series of oxygen and inorganic nutrient data off central Peru, Callao, spanning 16 years  
76 (1996-2011). The region of Callao has been identified as one of the major upwelling cells off central Peru (Rojas de Mendiola,  
77 1981) with a well-developed OMZ at subsurface (Wooster and Gilmartin, 1961; Zuta and Guillén, 1970). The presence of  
78 nitrate-rich ESSW (Zuta and Guillén, 1970; Strub et al., 1998; Graco et al., 2007; Silva et al., 2009) triggers the high primary  
79 production of the region, with maximum values in spring-summer, out of phase of winter upwelling maximum (Echevin et al.,  
80 2008; Chavez and Messié, 2009; Gutiérrez et al., 2011, Pennington et al., 2006; Vergara et al., 2016).

81 This dataset offers the opportunity to get insights in the ENSO oceanic teleconnection on the OMZ and nutrients  
82 features off the Peruvian upwelling system, considering recent advances in our understanding of ENSO events (Capotondi et  
83 al., 2015). The period under consideration encompasses characteristic events of the two ENSO regimes described by Takahashi

84 et al. (2011), that is a strong Eastern Pacific El Niño (i.e. the 1997-1998 strong El Niño) and a series of moderate Central  
85 Pacific El Niño events after 2000. Finally, the study explore the long-term trend from 1999 corresponding to a deepening of  
86 the oxygen deficient waters and a warming. Implications of our results for understanding the OMZ dynamics off Peru are  
87 discussed.

## 88 **2 Material and Methods**

### 89 **2.1 Study site and data**

90

91 The study site corresponds to a station off Callao (central Peru 12°02' S, 77°29' W, Fig. 1) located 20 nm from the coast and  
92 with 145 m water column depth. The station was visited most of the time by the Instituto del Mar del Peru (IMARPE) ship on  
93 a monthly or bimonthly basis between 1996 and 2011 to carry out vertical profiles of temperature, salinity, oxygen and nutrients  
94 (nitrate, nitrite, phosphate and silicate). Gaps larger than one or two months are however present over this period with the year  
95 2011 having 30% of missing data, which results in some limitations and require caution in processing the data and in  
96 interpreting the results (see section 2.2).

97 The temperature was measured by inversion thermometer through 2001 and by CTD (Seabird SBE 19+) from 2002.  
98 Salinity was measured by salinometer through 2001 and by CTD plus salinometer from 2002. Comparison between CTD  
99 measurements and estimates of temperature and salinity derived from water samples from the Niskin bottles were made  
100 regularly during all the cruises to verify the proper calibration of the instruments.

101 Dissolved oxygen and nutrients were measured most of the time at standard depths (0, 10, 30, 50, 75, 100 m). Dissolved  
102 oxygen was determined by a modified Winkler method (Grasshoff et al., 1999), with a precision of 0.5  $\mu\text{mol kg}^{-1}$ . Nutrient  
103 samples (nitrate, nitrite, phosphate and silicate) were frozen and stored before being analyzed using standard colorimetric  
104 techniques (Parsons et al., 1984). The estimated accuracy of the method was  $\pm 0.5 \mu\text{mol L}^{-1}$  for nitrate,  $\pm 0.08 \mu\text{mol L}^{-1}$  for  
105 nitrite,  $\pm 0.03 \mu\text{mol L}^{-1}$  for phosphate and  $\pm 0.25 \mu\text{mol L}^{-1}$  for silicate. Fixed nitrogen deficit (Ndef) was determined by the  
106 formula:

$$107 \text{Ndef} = 12.6 \times [\text{HPO}_4^{2-}] - ([\text{NO}_3^-] + [\text{NO}_2^-])$$

108 The constant 12.6 is the empirically-determined N:P ratio of organic matter produced in these waters (Codispoti and  
109 Packard, 1980). Positive values indicate nitrate deficit.

110 The OMZ was defined as the area with oxygen concentrations lower than 22.5  $\mu\text{mol kg}^{-1}$ . This concentration was considered  
111 as the OMZ upper boundary (Schneider et al., 2006; Fuenzalida et al., 2009; Ulloa and Pantoja, 2009).

### 112 **2.2 Statistical analysis of Time series**

113

114 The physical and chemical data off Callao showed missing monthly data, in particular the 2011 year that present up to 30% of  
115 the data missing. This is an inherent limitation of our data set that we have to take into account for the interpretation of the  
116 variability. In particular, the intra-seasonal variability (periods ranging from one month to 3-4 months) associated to the  
117 aliasing induced by the sampling of the data (i.e. one data point at best per month). Since the environmental conditions in the  
118 study region vary at daily to intra-seasonal time scales (Dewitte et al., 2011), the approximation that one measurement yields  
119 a monthly mean data may be biased. For this reason, the intra-seasonal variability in the data will not be documented in the  
120 paper that will focus on inter-annual time scales. As a consistency check and as an attempt to overcome such a limitation, we  
121 will use two methods to fill the gaps. First, the data were processed by linear interpolation in the vertical at each times step  
122 where data are available, then data either linearly interpolated in the time domain (first method) or using a 6-month running  
123 mean filter (second method). At least 2 data points within the 6-month windows are required, which leads to a data set without

124 gaps between January 1996 (data over 1995 are used to be able to start in January 1996 using such a filtering) and September  
125 2010. The latter procedure results in a low-pass filtering of the data so that aliasing and gridding artifacts are reduced compared  
126 to the first method. The first method is used to derive the oxycline and thermocline and second method is used to derive  
127 anomalies relative to a mean climatology. The latter is calculated from the raw data that have been only interpolated vertically  
128 at each time step on a regular grid (levels are 0, 10, 25, 50, 75 and 100 m). The period for the calculation of the climatology is  
129 1999-2011 (i.e. 13 years) but, due to the gaps in the time domain, each calendar month is calculated over a different number  
130 of years, always larger than 4 and lower than 12. The anomalies were calculated as the difference between the low-pass filtered  
131 data and the mean climatology. Wavelet analysis are performed on the time series and the global wavelet spectrum is derived  
132 (Torrence and Compo, 1998).

133 The Empirical Orthogonal Function (EOF) analysis (Thomson and Emery, 2014) was applied to the combined  
134 normalized time series of temperature, salinity, oxygen, inorganic nutrients, to extract the statistically dominant mode of  
135 covariability between the different components of OMZ dynamics (i.e. physical versus biogeochemical). The normalization  
136 of the time series consists in dividing them by their standard deviation. The analysis was performed taking into account the  
137 time series at all depths between 5m and 100m so that the statistics grasp some aspects of the vertical structure variability. The  
138 Pearson correlation coefficient ( $r$ ) was calculated between the data (or their PC time series) and some indices (see section 2.3)  
139 and the significance level of the correlation was estimated based on the degree of freedom inferred from the autocorrelation of  
140 the time series (i.e. taking the lag when it reaches zero the first time).

141 Long-term linear trend was calculated from the data that have been only interpolated vertically at each time step on  
142 the regular grid so that gaps in the time domain are considered in the estimate of the trend. They were calculated from January  
143 1999 to avoid an artifact associated with the strong 1997-1998 El Niño event. We tested whether the value of the slope is  
144 significantly different from 0 based on a Student's t-test. If the significance level is lower than 80%, the trend is considered  
145 not significant and only the slope values with confidence level larger than 90% are discussed.  
146

### 147 2.3 El Niño indices and Equatorial Kelvin Waves (EKW)

148  
149 In order to select the El Niño and La Niña years, we use the Oceanic El Niño Index (ONI) provided by the national Weather  
150 Service NOAA (NOAA, CPC. 2015). The magnitude of the events (weak, moderate, strong) are based on the ONI index, while  
151 the type of events (Eastern Pacific (EP) versus Central Pacific (CP) El Niño event) follows Yu and Kim (2013). This  
152 information is summarized in Table 1. To investigate the relationship between ENSO and the variability in the data, we use  
153 two other indices to account for the large-scale inter-annual variability in the equatorial Pacific. The two indices, named E and  
154 C, were defined by Takahashi et al. (2011), and account respectively for the Eastern Pacific El Niño events (hereafter EP  
155 events) and the Central Pacific El Niño events (hereafter CP events). These two indices are obtained from the first two PC  
156 time series of the EOF modes of the SST anomalies in the tropical Pacific (HadISST data set, Rayner et al.(2003)) over the  
157 period 1950-2014. Over the period of interest (1996-2011) the two indices are uncorrelated, so that they can be conveniently  
158 used as a basis over which the variability in the data can be projected. The projection onto the E index will account for the  
159 share of the variability in a particular field ( $T$ ,  $S$ ,  $O_2$ , Nitrate or Nitrite) that is associated to EP events, while the projection  
160 onto the C index will quantify the relationship between CP events and the variability in the data. An approximate temperature  
161 (similarly for  $S$ ,  $O_2$ , Nitrate and Nitrite) field can therefore be derived through bilinear regression analysis:  $T_{approx}(z,t)=$   
162  $\langle T(z,t)|E(t)\rangle \cdot E(t) + \langle T(z,t)|C(t)\rangle \cdot C(t)$ . It is expected that if there is a strong linear relationship with ENSO, the approximate  
163 data will explain a significant variance of the original data. However this may be not always the case for two reasons: 1) The  
164 relationship between ENSO and the variability in the data is not necessarily linear. 2) The coastal data are influenced by time  
165 scales of variability that are not necessarily accounted for by the E and C indices, since the latter are derived from SST which

166 is less variable than thermocline fluctuations (cf. Dewitte et al. (2008) for the equatorial region). In particular, Kelvin wave  
167 activity is enhanced several months prior to the ENSO peak (Mosquera et al., 2014) and the former can have a strong impact  
168 on the coastal circulation (cf. Ramos et al. (2008) for the 1997/98 El Niño event) although the ENSO peak is not already  
169 reached. That is why we will also use an estimate of the Equatorial Kelvin wave (EKW) activity to account for aspects of the  
170 remote forcing not necessarily contained in the E and C indices.

171 The estimate of the EKW was derived from an Ocean General Circulation Model (OGCM) simulation provided by  
172 Mercator, the European Institute for operational oceanography. The simulation has been validated from observations in recent  
173 previous studies (Mosquera-Vásquez et al., 2014), which indicates that, despite not assimilating observations, the simulation  
174 is as realistic as these SODA oceanic reanalysis (Carton and Giese, 2008) in the near-equatorial region over their overlapping  
175 period (1992-2008). The use of an OGCM simulation to derive the equatorial Kelvin wave is motivated by the possibility to  
176 estimate their vertical structure and separate waves having different propagating characteristics (phase speed and amplitude),  
177 which is not possible from observations. The method for deriving the wave coefficient consists in projecting the pressure and  
178 current anomalies from the model between 15°S and 15°N onto the theoretical vertical mode functions obtained from the  
179 vertical mode decomposition of the mean stratification. Kelvin wave amplitude is then obtained by projecting the results onto  
180 the horizontal modes at each grid point in longitude. The method has been shown to be successful in separating first and second  
181 baroclinic waves (Dewitte et al., 1999, 2008) that propagate at different phase speeds and impact the Peru coast in a very  
182 specific way (Illig et al., 2014). In particular, due to the sloping thermocline from west to east along the equator, the second  
183 baroclinic mode Kelvin wave tend to be more energetic and influential on the upwelling variability off the Peruvian coast  
184 (Dewitte et al., 2011, 2012). For the correlation analysis with the dissolved oxygen data, we select the EKW amplitude (in cm)  
185 for the first and second baroclinic modes (hereafter EKW\_1 and EKW\_2) at 90°W. Considering the phase speed of a coastal  
186 trapped-Kelvin wave (~250 km/days) this can be assumed as a good proxy of what happens off Callao in terms of wave activity.

## 187 **3 Results**

### 188 **3.1 Temperature and Salinity**

189  
190 The evolution of temperature and salinity off Callao over 1996-2011 as a function of depth is shown in Figure 2 a and b.  
191 Temperature and salinity experience significant temporal fluctuations at a wide range of time scales. Fluctuations,  
192 corresponding to near annual and inter-annual periods, are observed in the thermocline depth (15° C isotherm). Several  
193 deepening of the thermocline take place that correspond most of the time (but not always) to El Niño episodes and that are  
194 associated to enhanced salinity. There is in particular a strong deepening (more than 100m) of the 15°C isotherm between 1997  
195 and 1998 associated with significantly saltier waters over the water column (>35.1), which correspond to the signature of the  
196 strong 1997-1998 El Niño event. Note also that the disappearance of the 15°C isotherm in the upper 100 m that took place in  
197 early 1997 (around April), well ahead of the El Niño peak phase (around November). A slight deepening of the thermocline  
198 takes place also at the beginning of 2002, 2005, 2010 and during winter of 2006, 2008, 2009 and 2011. This thermocline  
199 deepening was coincident with high salinity values, clearly detected over the period 2002-2007.

200 The temperature data are further decomposed into a mean seasonal cycle and anomalies relative to this seasonal cycle  
201 (Figures 3 a and b). The latter is calculated over the period 1999-2011 in order to avoid a bias in the statistics due to the  
202 presence of the strong 1997-1998 El Niño. The mean seasonal cycle indicates that during austral winter and spring (June-  
203 August) colder conditions prevail in the water column, which is associated with less saline conditions (34.8-35.1). In particular,  
204 the 17°C isotherm outcrops between July and November. Note that during winter a slight deepening of the thermocline takes  
205 place as evidence by the evolution of the 15° C isotherm, while during spring the thermocline is shallower (up to 20 m). The

206 climatology also reveals the existence of a semi-annual component, which is thought to be related to the semi-annual cycle of  
207 the equatorial variability through oceanic teleconnection (Ramos et al., 2006).

208 The temperature and oxygen anomalies (Figure 3a) highlights the rich spectrum of variability as well as the  
209 differences between the strong 1997-1998 El Niño, a EP event and the subsequent periods. While temperature anomalies reach  
210  $\sim 5^{\circ}\text{C}$  at all depths during the 1997-1998 EP El Niño event, they are much weaker ( $\sim 1^{\circ}\text{C}$ ) for the following events and do not  
211 extend as deep. The period after 2000 corresponds to a period of dominant CP El Niño events that have a weaker amplitude  
212 than the 1997-1998 EP El Niño (Table 1), which explains the weaker temperature anomalies off Callao. A noticeable feature  
213 of the temperature anomalies after 1999 is also the existence of a long-term warming trend with a deepening of the  $15^{\circ}\text{C}$   
214 isotherm estimated to  $-0.30\text{ m decade}^{-1}$ . The analysis of the seasonality of the trend indicates that there is long-term deepening  
215 of the thermocline summer, spring and fall, while this is not the case in winter. The analysis of the trends (1999-2011) as a  
216 function of depth indicate that the warming takes place over the whole water column except at the surface (see Table 2).

### 217 3.2 Dissolved oxygen

218

219 The time series of dissolved oxygen over 1996-2011 off Callao exhibits a similar evolution than the thermohaline time series  
220 previously shown (Figure 2c) with large fluctuations at inter-annual scales. The strong 1997-1998 El Niño event is associated  
221 with the largest and deepest oxygenation event over the entire record ( $> 100\ \mu\text{mol kg}^{-1}$ ). A slight oxygenation in the water  
222 column takes place during 2002, 2006, 2008 2009 and 2011. This oxygenation is evidenced in the position of the oxycline  
223 (iso-oxygen of  $45\ \mu\text{mol kg}^{-1}$ ) and OMZ upper boundary ( $22.5\ \mu\text{mol kg}^{-1}$  iso-oxygen) depth.

224 The climatology of dissolved oxygen (Figure 3d) indicates a seasonal and semi-annual component, since the oxycline and  
225 OMZ upper boundary depth is shallower in summer- early fall (20-40 m) and spring (up to 20 m) and deeper in winter (50 m).  
226 Note that during summer-early fall and spring, oxygen-poor waters can intercept the euphotic layer and also the continental  
227 shelf, promoting suboxic and even anoxic conditions in bottom water underlying surface sediments ( $\text{O}_2 < 8.9\ \mu\text{mol kg}^{-1}$ ; Fig  
228 2c).

229 The time series of dissolved oxygen anomalies (Fig 3c) presents large positive oxygen anomalies during El Niño  
230 events, as the intense oxygen anomaly ( $> 60\ \mu\text{mol kg}^{-1}$ ) associated with the strong 1997-1998 El Niño when well-oxygenated  
231 Subtropical Surface Waters (SSW) occupied the upper 100 meters (Morón et al., 2000). The close relationship between the  
232 oxygen and thermocline depth during the 1997-1998 El Niño (i.e. positive  $\text{O}_2$  anomalies associated to a deepening of the  
233 thermocline) breaks down afterward for some events. Before 2000, the OMZ depth present a significant correlation with the  
234  $15^{\circ}\text{C}$  isotherm depth ( $r = 0.61$ ,  $v\text{-}p < 0.01$ ). After 2000, the correlation drops down ( $r = 0.28$ ,  $v\text{-}p < 0.01$ ).

235 The position of the OMZ upper limit shows a negative trend after 1999 with a deepening estimated to  $-0.64\text{ m decade}$   
236  $^{-1}$  (see Table 2) that points to a long-term deepening of the oxygen deficient waters, similar to the deepening trend of the  
237 thermocline depth for the same period. No significant difference appears in the seasonality of the OMZ trend (Table 2), contrary  
238 that the thermocline ( $15^{\circ}\text{C}$  depth) trend. The long-term trend (1999-2011) of oxygen concentration at different depths indicates  
239 a significant increase of oxygen in the entire water column. At surface, the increase is  $24.03\ \mu\text{mol kg}^{-1}\text{ decade}^{-1}$  (Table 2) while  
240 maximum trend is found in the first 25 m ( $47.55\ \mu\text{mol kg}^{-1}\text{ decade}^{-1}$ ).

241

### 242 3.3 Nutrients and biogeochemical activity

243

244 The time series of inorganic nutrient vertical distributions off Callao are shown in Figure 4. Nitrate and nitrite concentrations  
245 ranged from ca.  $0.0$  to  $27.0\ \mu\text{mol L}^{-1}$  and ca.  $0.2$  to  $9.0\ \mu\text{mol L}^{-1}$  respectively. Lower nitrate values are present at the surface (5  
246 m depth) and at deep waters ( $> 80\text{ m}$  depth), particularly during summer and fall periods, while maximum nitrite values appear

247 at subsurface waters in opposite relationship with nitrate levels. During winter, high nitrate concentrations are found in the  
248 entire water column ( $> 15 \mu\text{mol L}^{-1}$ ). The vertical distributions of silicate and phosphate exhibit a similar pattern than nitrate  
249 (not shown).

250 Nutrient data also present a strong inter-annual signal particularly during the strong 1997-1998 El Niño event with  
251 low nitrate concentrations ( $< 10 \mu\text{mol L}^{-1}$ ) coincident with minimum and even zero nitrite values and low silicate and phosphate  
252 levels ( $< 10 \mu\text{mol L}^{-1}$  and  $1 \mu\text{mol L}^{-1}$  respectively; Fig. 4). Between 1999 and 2001 nitrate concentrations were also lower than  
253  $10 \mu\text{mol L}^{-1}$  on average, but in contrast with the previous El Niño episodes, subsurface nitrite reached maximum values (up to  
254  $9 \mu\text{mol L}^{-1}$ ) coincident with an intense OMZ development and shallow thermocline (Fig. 2c).

255 Low silicate levels are registered at the sea surface, while silicate concentrations  $> 25 \mu\text{mol L}^{-1}$  associated with  
256 phosphate concentrations  $> 3 \mu\text{mol L}^{-1}$  are registered in subsurface waters. After 2000, subsurface nitrate concentrations  
257 reached the highest values ( $> 20 \mu\text{mol L}^{-1}$ ) over the entire record that is coincident with lower nitrite and silicate concentrations  
258 (Fig. 4). High nitrite pools in the water column were described as a typical feature under oxygen deficient waters (Deuser et  
259 al., 1978) and a tracer of denitrification (Codispoti and Packard, 1980; Codispoti and Christensen, 1985; Codispoti et al. 1986;  
260 1988) and anammox activity (Hammersley et al., 2007; Lam et al., 2009; Lam and Kuypers, 2011) off Peru.

261 In order to explore some biogeochemical activity related to the nitrogen cycle and the OMZ variability off Callao,  
262 Ndef in the water column is estimated (Fig. 5). Ndef values range from negative ( $-5 \mu\text{mol L}^{-1}$ ), indicative of low nitrate  
263 consumption, up to  $40 \mu\text{mol L}^{-1}$  corresponding to conditions of high nitrate deficiency. Ndef exhibits a clear inter-annual signal  
264 with minimum values (zero-negative) during the 1997-1998 El Niño event coincident with well-oxygenated waters (Fig. 2c).  
265 Low values of Ndef associated with almost zero nitrite concentrations suggest lower denitrification and/or anammox activity  
266 during these strong El Niño events. The significant effect on denitrification in the eastern South Pacific Ocean due to changes  
267 in the equatorial winds during El Niño was previously described by Codispoti et al. (1988). On the continental shelf off Callao,  
268 Dale et al. (2017), showed the occurrence of intra-annual and inter-annual variability in the denitrification and anammox  
269 processes that appears to decrease under El Niño coupled with low primary productivity and high bottom waters oxygenation.  
270 In contrast, between 1999 and 2001, Ndef of  $40 \mu\text{mol L}^{-1}$  peaked under a shallow and well-developed OMZ (Fig. 2c), pointing  
271 to nitrate reduction as an important route of organic matter remineralization yielding high nitrate concentrations at subsurface  
272 waters (Fig. 4).

273 After 2000, Ndef water column conditions were highly variable coincident with the variability in the OMZ  
274 distribution and in general a less intense OMZ. Intense nitrate deficient conditions were registered in 2005, 2007 and at the  
275 end of 2011 coincident with La Niña conditions (Table 1). Ndef at subsurface (50 and 90 m depth) was significantly correlated  
276 with the  $15^\circ\text{C}$  isotherm depth ( $r= 0.43$ ,  $v\text{-}p < 0.01$ ) and with the OMZ though the correlation is relatively low ( $r= 0.28$ ,  $v\text{-}p <$   
277  $0.01$ ). The Nitrate and Nitrite data do not exhibit a significant long-term trend from 1999 over the water column (See Table 2)  
278 although the post-2000 period has characterized by a reduction (increase) of nitrite (nitrate).

279

### 280 3.4 Equatorial forcing, Kelvin wave activity (EKW) and the OMZ off central Peru

281

282 As a first step, we document here the linear relationship between the variability in the data and ENSO taking into accounts its  
283 diversity (i.e. the existence of EP and CP El Niño events). This consists in regressing the data onto the E and C indices, which  
284 yields an approximate data that corresponds to the result of a statistical model where the E and C indices are predictors (see  
285 section 2). The regression coefficients for each data is presented in Figure 6 in dimensionalized unit, which provides the range  
286 of variations of a given field during a strong EP El Niño event (red curves in Fig. 6) and during a CP El Niño event (blue  
287 curves in Fig. 6). Note that the C index also accounts for the La Niña events so that the blue curves can be also interpreted as  
288 the variations of a particular field during a cold event. The Figure 6 reveals that variations in temperature, salinity and oxygen

289 during EP El Niño events are larger (~twice) than during CP El Niño event and of similar sign, consistently with the above  
290 description (Figures 2 and 3). The variation as a function of depth is also rather homogeneous, except for oxygen in the upper  
291 layer. In contrast, the variations for nitrate tend to have opposite signs and the amplitude during EP El Niño events is weaker  
292 in absolute value. The negative variation of nitrate during the EP El Niño events is consistent with the reduced upwelling  
293 during such events which results the deepening of the reach-nutrients cold coastal waters. In contrast, during CP El Niño  
294 events, nitrate concentration tends to increase consistently with the maintenance of upwelling conditions (see Dewitte et al.  
295 (2012)). During both EP and CP El Niño events, nitrite tends to decrease with depth in a similar way that could be explained  
296 by oxygen availability under both El Niño types.

297 The relevance of these results needs to be assessed in light of the variance explained by the statistical model, which  
298 is provided in Figure 7. The latter indicate a significant amount of variance explained by the linear statistical model for  
299 temperature and salinity (~30%). It is much less so for the biogeochemical fields, which could be due to two reasons: 1) there  
300 is a significant contribution of non-linear processes in the coupling between physics and biogeochemistry at ENSO time scales  
301 off Callao or/and, 2) the E and C indices do not account for all variability time Scales relevant for the oceanic teleconnection  
302 off Peru onto the biogeochemistry (i.e. equatorial Kelvin wave). In order to get further insights in the remote forcing of the  
303 OMZ, we thus document the evolution of EKW activity during 1996-2011. The evolution of the amplitude of the EKW\_1 and  
304 EKW\_2 at 90°W in terms of sea level anomalies is shown in the Figures 8a and b. These waves transmit their energy along  
305 the coast in the form of coastal trapped Kelvin waves and can trigger extra-tropical Rossby waves (Clarke and Shi, 1991). It  
306 is assumed that waves with amplitude larger than one standard deviation over the study period are downwelling Kelvin waves,  
307 whereas amplitudes more negative than -1 standard deviation correspond to upwelling Kelvin waves. The EKW\_2 activity is  
308 delayed by 1 month compared to EKW\_1, consistent with the difference in phase speed of the waves and their propagation  
309 from the central equatorial Pacific up to 90°W. Maximum correlation between both time series was before 2000 ( $r=0.67$ ,  $v-p<$   
310  $0.01$ ), being significantly lower after 2000 ( $r=0.42$ ,  $v-p<0.01$ ).

311 Positive anomalies of EKW are associated with a deepening of  $Z_{15^{\circ}\text{C}} (<0)$ , as was observed during the strong 1997-  
312 1998 El Niño, the weak 2002- 2003 El Niño and during 2006, 2008 and 2010 warm seasons. During these periods, EKW\_1  
313 and EKW\_2 are almost in phase with comparable amplitude and  $Z_{15^{\circ}\text{C}}$  and  $Z_{\text{OMZ}}$  (Fig. 8 d) are out of phase. The EKW\_1  
314 and EKW\_2 are highly correlated with  $Z_{15^{\circ}\text{C}}$  and  $Z_{\text{OMZ}}$  variables, but we find that EKW\_2 has a stronger relationship  
315 with the  $Z_{15^{\circ}\text{C}}$  and  $Z_{\text{OMZ}}$  ( $r -0.54$ ,  $-0.40$  respectively,  $v-p<0.01$ ) than EKW\_1 ( $r -0.34$ ,  $-0.23$  respectively,  $v-p<0.01$ ).  
316 The global wavelet spectrum of the EKW\_1 and EKW\_2 time series at 90°W show that the second baroclinic mode is  
317 associated with lower frequency variability than the first baroclinic Kelvin wave mode (Fig. 8 a, b). It is noteworthy that  
318 EKW\_2 is negatively skewed since 2000 (normalized skewness =  $-0.8910$  cm) and there is a negative trend of upwelling events  
319 since 2000 (trend =  $-0.0177$  cm/decade), features that are also encountered for  $Z_{15^{\circ}\text{C}}$  (Fig. 8 c) (normalized skewness =  $-$   
320  $1.330$  m and trend =  $-0.30$  m decade<sup>-1</sup>). The global wavelet spectra for  $Z_{15^{\circ}\text{C}}$  and  $Z_{\text{OMZ}}$  (Fig. 8 h, i) also reveal a rich  
321 spectrum of variability that is characterized by a double peak, one at ~4 years and the other one near 2.2 years. N def at 50 m  
322 (Fig. 8 d) exhibits a spectrum with a single dominant peak at ~4 years. Summarizing, the spectral analysis of the synthetic  
323 proxies for the physical (EKW,  $Z_{15}$ ) and biogeochemical ( $Z_{\text{OMZ}}$ , Ndef at 50m) processes suggests that coupling between  
324 physics and biogeochemistry in relation with ENSO may take place at various time scales.

325 As an attempt to quantify such a coupling and its relationship with the remote forcing, an EOF analysis is performed  
326 combining all the data (temperature, salinity, oxygen, nitrate and nitrite) (see section 2 for details). The EOF analysis is  
327 performed over two periods, 1996-2010 and 1999-2010 to differentiate the coupling characteristics as a function of the El Niño  
328 types considering that the 1997-1998 EP El Niño event is very influential on the obtained statistics. The results of the EOF  
329 analysis are presented in Figure 9 for the first and second EOF modes (EOF1 and EOF2). The PC time series for the period  
330 1996-2010 indicate that the EOF1 mode mostly captures the variability (43%) associated to the strong 1997-1998 El Niño  
331 event (with a high correlation between PC1 and the E index, see Table 3), while the EOF2 mode explains 18% of the variance



332 and does not relate to any particular events or series of events. The latter is confirmed by the low correlation between PC2 and  
333 the E (or C) index (see Table 3). The EOF2 thus captures the share of the coupled variability that is not linearly related to the  
334 remote ENSO forcing, which is also supported by the low correlation between PC2 and the EKW time series (see Table 3).  
335 This is independent of the periods over which the EOF analysis is performed. For the 1999-2010 period the EOF analysis (Fig.  
336 9 d, e, f) indicates significant distinct characteristics than the EOF modes obtained for the entire period. In particular, the PC1  
337 time series is highly correlated to the C index when the EOF analysis is performed without including the 1997-1998 El Niño  
338 event, which indicates that the dominant EOF modes over the two periods capture the share of the coupled variability that is  
339 related to the different El Niño types. The patterns of EOF1 for the two periods (Figs. 9 b, e) are comparable for temperature,  
340 salinity and oxygen, that is, a strong positive loading over most of the water column. Differences can be observed at the surface  
341 for oxygen, where the loading of the EOF1 mode pattern over 1996-2010 is weaker near the surface compared to the period  
342 1999-2010. This could be related to the strong warming of the mixed-layer during the 1997-1998 El Niño event that leads to  
343 reduced solubility of oxygen and compensates for the downwelling-induced oxygenation. Differences in mode patterns  
344 between the two periods are more pronounced for nitrate and to a lesser extent for nitrite. In particular, the nitrate profile  
345 exhibits a bend near 30m for the period 1996-2010 that is more marked than for the period 1999-2010. Differences in mode  
346 patterns between the two periods are emphasized for mode EOF2 (Figs. 9 c, f), which is difficult to interpret. Note that the  
347 oxygen profiles have an opposite sign between the two periods, which suggests a completely different coupled dynamics  
348 associated to the “natural” mode of variability. Overall the results of the EOF analysis suggest two different regimes of the  
349 coupling between physics and biogeochemistry over the two periods, which is associated to the El Niño types. A “strong”  
350 regime associated to the strong 1997-1998 EP El Niño event and a “weak” regime corresponding to the subsequent period  
351 where the environmental forcing consists in the alternation of CP El Niño events and La Niña events and the enhanced EKW  
352 activity. The coupling efficiency (i.e. “strong” versus “weak”) is provided by the amplitude of the mode patterns (Figs 9 b,e),  
353 and to some extent by the percentage of variance of EOF1, 43% for the period 1996-2010 and 37% for the period 1999-2010.

354 The EOF analysis also indicate that the “forced” (i.e. by ENSO) coupled variability (EOF1) is related to ENSO  
355 through the forcing of the second baroclinic mode Kelvin wave as evidenced by the large positive correlation between EKW\_2  
356 and PC1 for the two periods (Table 3). The EOF2 mode does not exhibit any linear relationship with ENSO and may account  
357 for the large natural variability of the coastal system and/or higher-frequency environmental forcing (e.g. internal waves, intra-  
358 seasonal variability from oceanic or atmospheric origin) that can rectify on the circulation at inter-annual time scales. For  
359 instance, intra-seasonal Kelvin wave forcing may trigger changes in the circulation along the coast (Illig et al., 2014) that  
360 subsequently acts on the biogeochemistry through non-linear dynamics (Vergara et al., 2016). Due to limitations in the data  
361 set, it is difficult to address this issue that would require the experimentation with a regional coupled model. This is beyond  
362 the scope of the present study.

363

#### 364 **4 Discussion and concluding remarks**

365

366 The data of temperature, salinity, oxygen and nutrients between 1996 and 2011 in the central area of the Peruvian upwelling  
367 system reveal a rich spectrum of variability. The record encompasses one of the few strong Equatorial Pacific (EP) El Niño  
368 events observed over the last five decades and the series of Central Pacific (CP) El Niño events of the 2000s, which allows  
369 documenting the OMZ dynamics under two different ENSO regimes and thus extends a previous study (Gutiérrez et al., 2008).  
370 Our analysis reveals two contrasting biogeochemical regimes associated to the two El Niño types. During “strong” regimen  
371 (strong 1997-1998 EP El Niño events), the biogeochemical properties are largely constrained by the wave-induced  
372 downwelling conditions reflected on extreme oxygenation, reduced nutrients availability and decrease nitrogen lost processes  
373 (denitrification, anammox). During the “weak” (CP El Niño events), less intense downwelling conditions determine a less  
374 intense OMZ (oxygen concentration increase weakly), higher nitrate concentration and nitrogen lost processes appear not to

375 be significant. While under the 1997-1998 EP El Niño the biogeochemical activity was clearly coupled to the physical forcing,  
376 this was not evident during the dominant CP El Niño regime. This reflects the distinct oceanic teleconnection through the  
377 equatorial Kelvin waves in which mean upwelling conditions are hardly altered during the CP El Niño events (Dewitte et al.,  
378 2012). The interpretation of the variability in these two regimes is consistent with the results of our EOF analysis combining  
379 physical and biogeochemical data (Figure 9) which indicates that the statistics (explained variances of the modes and mode  
380 patterns) are modified whether or not the 1997-1998 El Niño event is considered in the analysis. In particular, whereas the  
381 dominant EOF mode that relates to the ENSO remote forcing explains less variance when the 1997-1998 El Niño is not  
382 considered in the analysis, the second EOF mode that is independent of ENSO, exhibits a drastic change in the mode patterns  
383 for oxygen, nitrite and nitrate. This second mode can be interpreted as resulting from the natural variability of the coupled  
384 system, that is, the variability associated to non-linear processes in the biogeochemical system or to residual effect of other  
385 oceanic processes (e.g. eddy activity) on the mean circulation (i.e. rectification processes). The existence of a “natural”  
386 variability in the OMZ is suggested by regional model simulations (Bettencourt et al., 2015; Vergara et al., 2016). Our results  
387 propose that such natural variability would be larger over periods when the frequency of CP El Niño events occurrence would  
388 be larger than the one of EP El Niño event.

389         The data set also offers the opportunity to explore longer timescales of variability. Our analysis in particular suggests  
390 a negative trend in oxygen concentration associated to a warming over the period 1999-2011. This is in contrast with the long-  
391 term deoxygenation trend over the last decades in the eastern tropical Pacific by Stramma et al. (2008; 2010). This suggests  
392 that either the low-frequency oxygen variability off Callao is not representative of the low-frequency changes of the off-shore  
393 OMZ or that the trend in our data is associated to decadal changes (since it is estimated over only 13 years). This would deserve  
394 further investigation in order to reconcile observations in the off-shore ocean and at the coast off Peru. The other striking  
395 feature in our data set is that only temperature and oxygen experience a significant trend from 1999 (See Table 2). While the  
396 interpretation of the latter remains uncertain, it is consistent with the existence of a significant natural variability since trend  
397 could also emerge from non-linear processes embedded into the biogeochemical coupled system. The better understanding of  
398 the natural variability would certainly benefit from the experimentation with a regional coupled model, which need take in  
399 account for future work.

400         We now discuss some limitations of our analysis. First, our interpretation of the OMZ variability does not consider  
401 aspects of the wind forcing, although the latter is highly variable in the central Peru region and is influential on the upwelling  
402 dynamics. While during El Niño events, there is, in general a weakening of the upwelling favorable winds at regional scale  
403 due to the relaxation of the South Eastern branch of the trade winds, near the coast winds can intensify locally because of  
404 underlying warm waters effect (Dewitte and Takahashi, 2017). To which extent such anomalous winds influence the local  
405 oceanic circulation and associated biogeochemical response remains to be investigated. Considering the limited knowledge on  
406 this aspect and limitations in the wind data sets (Goubanova et al., 2011), we have not introduced the analysis of the local wind  
407 forcing at inter-annual timescale here. However, this issue certainly deserves further investigation. Another important  
408 limitation of our study is associated to the sampling of the data. The latter may result in an aliasing of the high-frequency  
409 fluctuations embedded into the environmental forcing (i.e. intra-seasonal Kelvin wave and winds, cf. Dewitte et al. (2011))  
410 into the low frequency fluctuations and may bias the estimate of the low-frequency mode. Gridding procedure to fill in gaps  
411 in the data can also introduce unrealistic timescales of variability. We have here confronted two gridding procedures (one  
412 based on simple low-pass filtering and other using a 6-month running mean filter) and they qualitatively lead to comparable  
413 results in terms of the inter-annual and long-term variability. It would be interesting to quantitatively assess the effect of the  
414 aliasing of high frequencies onto the monthly mean based on observations. The use of a long-term regional coupled model  
415 simulation would be also valuable for addressing this issue. The latter could in particular allows investigating the remote  
416 oceanic forcing associated to the intra-seasonal Kelvin wave on the oxygen conditions off Peru, which was not possible from  
417 our data set. It could also help in better understanding how the intra-seasonal variability can rectify on the inter-annual

418 variability through non-linear processes (e.g. eddy transport). Despite these limitations, the results presented in this paper are  
419 valuable as a benchmark for the validation of regional coupled models that are aimed to address the OMZ dynamics.

420 Overall, our results illustrate the rich spectrum of OMZ variability at inter-annual timescales, which cannot be solely  
421 interpreted as resulting from the ENSO oceanic teleconnection. Natural variability in the OMZ is expected from the complex  
422 of processes involved. Our analysis provides a first assessment of such a variability from observations. Understand the intensity  
423 and distribution of the OMZ is essential to understand changes in nutrients and finally to predict the productivity and  
424 distribution of marine resources. The existence of the two regimes suggested here need to be tested from global or regional  
425 models, which could provide a pathway for understanding the sensitivity of the OMZ to climate variability and for a better  
426 prediction of global change scenarios.

427

#### 428 ***Acknowledgements***

429 This research was supported by the Instituto del Mar del Peru (IMARPE). We thank Carlos Robles and Miguel Sarmiento, the  
430 technical chemical staff. Thanks to the crew of the IMARPE VIII and the SNP-2 research vessels and all the scientific  
431 colleagues that help us. This work is a contribution of the project “Integrated Study of the Upwelling system off Peru”  
432 developed by the first author in the Direction of Oceanography and Climate Change Research of IMARPE. Boris Dewitte  
433 acknowledges support from FONDECYT (project 1151185) and IRD. Mercator is thanked for providing the model data to  
434 derive the Kelvin wave estimate. We are grateful to the two anonymous reviewers for their constructive comments that helped  
435 to improve the manuscript. This work is a contribution of the project “Integrated Study of the Upwelling system off Peru”  
436 developed in the Direction of Oceanography and Climate Change Research of IMARPE.

#### 437 **References**

- 438 Ashok, K., S. K. Behera, S. A., Rao, H. Weng, and Yamagata, T.: El Niño Modoki and its possible teleconnection, *J. Geophys.*  
439 *Res.*, 112, C11007, doi:10.1029/2006JC003798, 2007.
- 440 Bertrand A, M. Ballón, and Chaigneau, A.: Acoustic observation of living organisms reveals the upper limit of the oxygen  
441 minimum zone. *PLoS ONE*, 5(4), E10330, doi:10.1371/journal.pone.00103330, 2010.
- 442 Bettencourt J., Lopez, C., Hernandez-Garcia, E. Montes, I. Sudre, J. Dewitte, B., Paulmier A. and Garçon, V.: Boundaries of  
443 the Oxygen Minimum Zone shaped by coherent mesoscale dynamics. *Nature Geoscience*, doi:10.1038/NGEO2570,2015.
- 444 Calienes, R., and Guillén, O.: Masas de agua y producción primaria en el Perú. *Bol. Inst. Mar Perú*, Vol. Extraordinario  
445 ICANE, 155-163, 1981.
- 446 Calvert, S.E., and Price, N.B.: Recent sediments of the South West Africa shelf, in *The Geology of the East African Continental*  
447 *Margin*: Delany, E. M. (Ed.): Univ. Edinburg. *Inst. Geol. Sci. Rept.* 70, 16, 171-185, 1971.
- 448 Capotondi A., Wittenberg, A., Newman, M., Di Lorenzo, E., Yu, J.-Y., Braconnot, P. Cole, J., Dewitte, B., Giese, B., Guilyardi,  
449 E., Jin, F.-F., Karnauskas, K., Kirtman, B., Lee, T., Schneider, N., Xue, Y. and Yeh, S.-W.: Understanding ENSO diversity.  
450 *Bull. Amer. Met. Soc.* doi.: 10.1175/BAMS-D-13-00117.1. 2015.
- 451 Carton, J.A., and Giese, B.S.: A reanalysis of ocean climate using Simple Ocean Data Assimilation (SODA), *Mon. Wea. Rev.*,  
452 136, 2999-3017, 2008.
- 453 Chavez, F.P., Bertrand, A., Guevara-Carrasco, R., Soler, P. and Csirke, J.: The northern Humboldt Current System: brief  
454 history, present status and a view towards the future. *Prog. Oceanogr.*, 79: 95-105, 2008.
- 455 Chavez, F., and Messié, M.: A comparative analysis of eastern boundary upwelling ecosystems. *Prog Oceanogr.* 83, 80–96,  
456 2009.
- 457 Clarke, A. J.: The reflection of equatorial waves from oceanic boundaries. *J. Phys. Oceanogr.*, 13, 1193 – 1207, 1983.

458 Clarke, A.J. and Shi, C.: Critical frequencies at ocean boundaries. *Journal of Geophysical Research* 96: doi:  
459 10.1029/91JC00933. issn: 0148-0227, 1991.

460 Clarke A., and van Gorder, S.: On ENSO coastal currents and sea level. *J. Phys. Oceanogr.*, 24, 661–680, 1994.

461 Codispoti, L.A., and Packard, T.T.: Denitrification rates in the eastern tropical South Pacific. *J. Mar. Research*, 38, 453-477,  
462 1980.

463 Codispoti, L.A., and Christensen, J.P.: Nitrification, denitrification and nitrous oxide cycling in the eastern tropical South  
464 Pacific Ocean. *Mar. Chem.*, 16, 277-300, 1985.

465 Codispoti, L.A., G. Friederich, T.T. Packard, H.E. Glover, P.J. Kelly, R.W. Spinrad, R. T. Barber, W. Elkins, B.B. Ward, F.  
466 Lipschultz, and Lostanau, N.: High nitrite levels off northern Perú. A signal of instability in the marine denitrification rate.  
467 *Science*, 233, 1200-1202, 1986.

468 Codispoti, L.A., G. Friederich, T.T. Packard, and Barber, B.B.: Remotely driven thermocline oscillations and denitrification  
469 in the Eastern South Pacific: The potential for high denitrification rates during weak coastal upwelling. *The Sci. of the Total*  
470 *Environment*, 75, 301-318, 1988.

471 Criales-Hernández, M. I., M. Graco, P. Ayón, G. Flores, R. Schwaborn, H.-J. Hirche, and Wolff, M.: Temporal variability  
472 of the mesozooplankton community in the Humboldt upwelling system off central Peru. *Extended Abstracts. International*  
473 *Conference The Humboldt Current System: Climate, ocean dynamics ecosystem processes and fisheries*, Lima, November 27  
474 December, 1, 151, 2006.

475 Dale AW, Graco M and Wallmann K (2017) Strong and Dynamic Benthic-Pelagic Coupling and Feedbacks in a Coastal  
476 Upwelling System (Peruvian Shelf). *Front. Mar. Sci.* 4:29. doi: 10.3389/fmars.2017.00029.

477 Deuser, W. G., Ross, E. H., and Mlodzinska, Z. J.: Evidence for and rate of denitrification in the Arabian Sea. *Deep-Sea Res.*,  
478 25, 431-445, 1978.

479 Dewitte B., G. Reverdin, and Maes, C.: Vertical structure of an OGCM simulation of the equatorial Pacific Ocean in 1985-  
480 1994. *J. Phys. Oceanogr.*, 29, 1542-1570, 1999.

481 Dewitte B., S. Illig, L. Parent, Y. duPenhoat, L. Gourdeau and J. Verron,: Tropical Pacific baroclinic mode contribution and  
482 associated long waves for the 1994-1999 period from an assimilation experiment with altimetric data. *J. Geophys. Research.*,  
483 08 (C4), 3121-3138, 2003.

484 Dewitte B., S. Purca, S. Illig, L. Renault, and Giese, B.: Low frequency modulation of the intra-seasonal equatorial Kelvin  
485 wave activity in the Pacific ocean from SODA: 1958-2001. *J. Climate*, 21, 6060-6069, 2008.

486 Dewitte, B., S. Illig, L. Renault, K. Goubanova, K. Takahashi, D. Gushchina, K. Mosquera-Vásquez, and Purca, S.: Modes of  
487 covariability between sea surface temperature and wind stress intra-seasonal anomalies along the coast of Peru from satellite  
488 observations (2000-2008). *J. Geophys. Research*, 116, C04028, doi:10.1029/2010JC006495, 2011.

489 Dewitte B., J. Vazquez-Cuervo, K. Goubanova, S. Illig, K. Takahashi, G. Cambon, S. Purca, D. Correa, D. Gutiérrez, A.  
490 Sifeddine, and Ortlieb, L.: Change in El Niño flavors over 1958-2008: Implications for the long-term trend of the upwelling  
491 off Peru. *Deep Sea Research II*, 123-135, 2012.

492 Dewitte B. and K. Takahashi: Diversity of moderate El Niño events evolution: role of air-sea interactions in the eastern  
493 tropical Pacific. *Climate Dynamics*, revised. , 2017.

494 DIVA 2017. Latest ODV4 Version: ODV4.7.10 (Feb 07 2017).

495 Echevin, V., Aumont, O., Ledesma, J., and Flores, G.: The seasonal cycle of surface chlorophyll in the Peruvian upwelling  
496 system: A modeling study. *Progr. Oceanogr.* 72, 167-168, 2008.

497 Ekau, W., H. Auel, H.-O. Portner, and Gilbert, D.: Impacts of hypoxia on the structure and processes in pelagic communities  
498 (zooplankton, macro-invertebrates and fish. *Biogeosciences*, 7, 1669–1699, doi:10.5194/bg-7-1669-2010, 2010.

499 Franz, J., Krahnemann, G., Lavik, G., Grasse, P., Dittmar, T., and Riebesell, U.: Dynamics and stoichiometry of nutrients and  
500 phytoplankton in waters influenced by the oxygen minimum zone in the eastern tropical Pacific, *Deep-Sea Res. Pt. I*, 62, 20–  
501 31, 2012.

502 Friederich, G., Ledesma, J., O. Ulloa, and Chavez, F.: Air-sea carbon dioxide fluxes in the coastal southeastern tropical Pacific.  
503 *Progr. Oceanogr* 72, 156-166, 2008.

504 Fuenzalida R, W. Schneider, J. Garcés-Vargas, L. Bravo, and Lange, C.: Vertical and horizontal extension of the oxygen  
505 minimum zone in the eastern South Pacific Ocean. *Deep Sea Res. II*, 56,1027–1038, 2009.

506 Furue, R., McCreary, J.P., Yu, Z. and Wang, D.: The dynamics of the southern Tsuchiya Jet, *J. Phys. Oceanogr.*, 37, 531-553.  
507 2007.

508 Goubanova K., V. Echevin, B. Dewitte, F. Codron, K. Takahashi, P. Terray, M. Vrac, 2011: Statistical downscaling of sea-  
509 surface wind over the Peru-Chile upwelling region: diagnosing the impact of climate change from the IPSL-CM4 model. *Clim.*  
510 *Dyn.*, DOI 10.1007/s00382-010-0824-0.

511 Graco, M.I., J. Ledesma, G. Flores, and Girón, M.: Nutrientes, oxígeno y procesos biogeoquímicos en el sistema de surgencias  
512 de la corriente de Humboldt frente a Perú. *Rev. Biol. Peruana* 14 (1): 117-128, 2007.

513 Grasshoff, K., M. Ehrhardt, K. Kremling, and Anderson, L.G.: *Methods of seawater analysis*. Wiley, 1999.

514 Guillén, O., and Izaguirre de Rondán, R.: Nutrients in the Perú coastal current. In *Oceanography of the South Pacific 1972*,  
515 Ed. R. Fraser, National commission for UNESCO, 397-418, 1973.

516 Guillén, O. G., E.A. Cárcamo, and Calienes, R.: Oxígeno disuelto, nutrientes y clorofila frente a la costa peruana durante el  
517 Niño 1987. *Bol. Imarpe, Vol. Especial*, 83-94, 1989.

518 Gutiérrez, D., Enríquez, E., Purca, S., Quipuzcúa, L., Marquina, R., Flores G., and Graco, M.: Oxygenation episodes on the  
519 continental shelf of central Peru: remote forcing and benthic ecosystem response. *Prog. Oceanogr.* 79, 177–189, 2008.

520 Gutiérrez, D., Bouloubassi, I., Sifeddine, A., Purca, S., Goubanova, K., Graco, M., Field, D., Mejanelle, L., Velazco, F., Lorre,  
521 A., Salvatelli, R., Quispe, D., Vargas, G. Dewitte, B. and Ortlieb, L.: Coastal cooling and increased productivity in the main  
522 upwelling zone off Peru since the mid-twentieth century. *Geophys. Res. Lett.* 38, L07603, 2011.

523 Hammersley, M.R., Lavik, G., Woebken, D., Rattray, J.E., Lam, P., Hopmans, H., Sinninghe Damsté, J.S., Kruger, S., Graco,  
524 M., Gutiérrez D., and Kuypers, M.: Anaerobic ammonium oxidation contributes significantly to nitrogen loss from the  
525 Peruvian oxygen minimum zone. *Limnol. Oceanogr.* 52(3), 923-933, 2007.

526 Helly, J.J., and Levin, L.A.: Global distribution of naturally occurring marine hypoxia on continental margins. *Deep-Sea*  
527 *Research Part I*, 51, 1159-1168, 2004.

528 Illig S., B. Dewitte, K. Goubanova, G. Cambon, J. Boucharel, F. Monetti, C. Romero, S. Purca and R. Flores.: Forcing  
529 mechanisms of intra-seasonal SST variability off Peru in 2000-2008: local versus remote forcings. *J. Geophys. Res.-Oceans*,  
530 Vol. 119, 6, 3548-3573, 2014.

531 Kock, A., Arévalo-Martínez D., Loscher, C. and Bange, H.: Extreme N<sub>2</sub>O accumulation in the coastal oxygen minimum zone  
532 off Perú, *Biogeoscience*, 13, 827-840, doi:10.5194/bg-13-827-2016, 2016.

533 Lam, P., Lavik, G., Jensen, M.M., van de Vossenburg, J., Schmid, M.C., Woebken, D., Gutiérrez, D., Aman, R., Jetten, M.S.M.  
534 and Kuypers, M.: Revising the nitrogen cycle in the Peruvian oxygen minimum zone. *P. Natl. Acad. Sci. USA*, 106, 4752–  
535 4757, 2009.

536 Lam, P. and Kuypers, M.: Microbial Nitrogen Cycling Processes in Oxygen Minimum Zones. *Annu. Rev. Mar. Sci.* 3,317–  
537 45, 2011.

538 Ledesma, J., Tam, J., León, V., Flores, G., & Morón, O.: Caracterización de la Zona de Mínimo de Oxígeno (ZMO) frente a  
539 la costa peruana entre 3° N y 14° S, 1999-2009. Informe Instituto del Mar del Perú Volumen 38, N°1. 2011

540 Lee, T., and McPhaden, M. J.: Increasing intensity of El Niño in the central-equatorial Pacific, *Geophys. Res. Lett.*, 37, L14603,  
541 doi:10.1029/ 2010GL044007, 2010.

542 Levin, L., Gutiérrez, D., Rathburn, T., Neira, C., Sellanes, J., Muñoz, P., Gallardo, V. and Salamanca, M.: Benthic processes  
543 on the Peru margin: a transect across the oxygen minimum zone during the 1997–98 El Niño. *Prog. Oceanogr.*,53,1-27,2002.

544 Montes, I., Colas, F., Capet, X., and Schneider, W.: On the pathways of the equatorial subsurface currents in the eastern  
545 equatorial Pacific and their contributions to the Peru-Chile Undercurrent. *J. Geophys. Research.*,  
546 115,C09003,doi:10.1029/2009JC005710,2010.

547 Morales, C.E., Hormazábal, S.E., and Blanco, J.L.: Inter-annual variability in the mesoscale distribution of the depth of the  
548 upper boundary of the oxygen minimum layer off northern Chile (18-24S): Implications for the pelagic system and  
549 biogeochemical cycling. *J. Mar. Res.*,57,909-932,1999.

550 Morón, O.: Características del ambiente marino frente a la costa peruana. *Bol. Inst. Mar Perú*, 19 (1:2), 179-204, 2000.

551 Morón O., and Escudero L.: Salinidad promedio de la superficie del mar frente a la costa peruana. Período 1928-1985. Internal  
552 Report. IMARPE, 1991.

553 Mosquera-Vásquez, K., Dewitte, B., and Illig, S.: The central Pacific El Niño intra-seasonal kelvin wave JGR: *Oceans*.  
554 10.1002/2014JC10044, 2014.

555 NOAA CPC. Oceanic El Niño Index (ONI) [http://www.cpc.noaa.gov/products/analysis\\_monitoring](http://www.cpc.noaa.gov/products/analysis_monitoring), 2015.

556 Parsons, T. R., Maita, Y., and Lalli, C.M.: A manual of chemical and biological methods for seawater analysis, Pergamon  
557 Press, Oxford, UK, 173 pp, 1984.

558 Paulmier, A. and Ruiz-Pino, D.: Oxygen minimum zones in the modern ocean. *Prog. Oceanogr.* 80, 113-128, 2009.

559 Pennington, J. T., Mahoney, K.L., Kuwahara, V.S., Kolber, D.D., Calienes, R., and Chavez, F.: Primary Production in the  
560 eastern tropical Pacific: a review. *Prog. Oceanogr.*, 69 (2-4), 285-317, 2006.

561 Ramos, M., Pizarro, O., Bravo, L., and Dewitte, B.: Seasonal variability of the permanent thermocline off northern Chile.  
562 *Geoph. Res. Lett.*, 33, L09608, doi:10.1029/2006GL025882, 2006.

563 Ramos, M. Dewitte, B., Pizarro, O. and Garric, G.: vertical propagation of extratropical Rossby waves during the 1997-1998  
564 El Niño of the west coast of South America in a medium resolution OGCM simulation. . *J. Geophys. Research.*, 113 (C8041),  
565 doi: 10.1029/2007JC004681, 2008.

566 Rayner, N. A., D. E. Parker, E. B. Horton, C. K. Folland, L. V. Alexander, D. P. Rowell, E. C. Kent, and A. Kaplan,: Global  
567 analyses of sea surface temperature, sea ice, and night marine air temperature since the late nineteenth century, *J. Geophys.*  
568 *Res.*, 108(D14), 4407, doi:10.1029/2002JD002670, 2003.

569 Rojas de Mendiola, B.: Seasonal phytoplankton distribution along the peruvian coast, in: *Coastal Upwelling*, F. A. Richards  
570 (Ed.), American Geophysical Union, 348-356 pp., 1981.

571 Sánchez, G., Calienes, R., and Zuta, S.: The 1997-1998 El Niño and its effect on the marine coastal system off Perú. CALCOFI  
572 reports, 41, 62-86, 1999.

573 Schneider, W., Fuenzalida, R., Garcés-Vargas, J., Bravo, L., and Lange, C.: Extensión vertical y horizontal de la zona de  
574 mínimo de oxígeno en el pacífico Sur oriental. Extended Abstract. *The Oxygen Minimum Systems in the ocean: Distribution,*  
575 *Diversity and Dynamics Workshop*, Concepción, Chile., October 24-26. *Suplemento Gayana*, 70, 79-82, 2006.

576 Silva, N., N. Rojas, and Fedele, A.: Water masses in the Humboldt Current System: Properties, distribution, and the nitrate  
577 deficit as a chemical water mass tracer for Equatorial Subsurface Water off Chile. *Deep-Sea Res. Pt. II*, 56, 1004-1020, 2009.

578 Stramma, L., Johnson, G.C., Sprintall, J., and Mohrholz, V.: Expanding oxygen-minimum zones in the tropical oceans.  
579 *Science*. 320, 655-658, 2008.

580 Stramma, L., Schmidtko, S., Levin, L., and Johnson, G.C.: Ocean oxygen minima expansions and their biological impacts.  
581 *Deep-Sea Res. Pt. I: Oceanographic Research Papers*, 57(4): 587-595, 2010.

582 Strub, P. T., Mesías, J.M., Montecino, V., Rutlant, J., and Salinas, S.: Coastal ocean circulation off western South America.  
583 *Coastal Segment (6, E)*, in *The Sea*, A. R. Robinson and K. H. Brink (Eds.), Wiley, 273-313 pp., 1998.

584 Takahashi, K., Montecinos, A., Goubanova, K., and Dewitte, B.: ENSO regimes: Reinterpreting the canonical and Modoki El  
585 Niño. *Geoph. Res. Lett.*, 38, L10704, doi:10.1029/2011GL047364, 2011.

586 Thomson, R.E., and Emery, W.J.: *Data analysis methods in physical oceanography*, Third edition, Elsevier. 187-191,425-536,  
587 2014.

588 Torrence, C., and Compo, G.P.: A practical guide to wavelet analysis. *Bul. Am. Meteorol. Soc.*, 79, 61–78, 1998.

589 Ulloa, O and Pantoja, S.: The oxygen minimum zone of the eastern South Pacific. *Deep-Sea Res. Pt. II*, 56, 987–991, 2009.

590 Vergara, O., B. Dewitte, I. Montes, V. Garçon, M. Ramos, A. Paulmier, and O. Pizarro: Seasonal Variability of the Oxygen  
591 Minimum Zone off Peru in a high-resolution regional coupled model. *Biogeosciences*. 13, 4389-4410, 2016.

592 Wooster, W. S., and Gilmartin, M.: The Peru-Chile Undercurrent. *J. Mar. Research*, 19, 97-122, 1961.

593 Wyrtki, K.: The oxygen minima relation to ocean circulation. *Deep-Sea Res.*, 9, 11-23, 1962.

594 Yeh, S.-W., Kug, J.-S., Dewitte, B., Kwon, M.-H., Kirtman, B.P., and Jin, F.-F.: El Niño in a changing climate, *Nature*, 461,  
595 511–515, 2009.

596 Yu, J.I. and S.-T Kim, :Identifying the types of major El Niño events since 1870, *Int. J. Climatol.* 33(8), 2015-2112, 2013.

597 Zuta, S., and Guillén, O.G.: *Oceanografía de las aguas costeras del Perú*. *Bol. Inst. Mar Perú*, 2, 157-324, 1970.

598

600 **Table 1: El Niño and La Niña years and their characteristics (magnitude and type)**

El Niño (red) and La Niña (blue) years	Magnitude (ONI index)	Type (Eastern Pacific -EP versus Central Pacific-CP) (Yu and Kim, 2013)
1997/1998	Strong (extraordinary)	EP
1998/1999	moderate	
1999/2000	moderate	
2000/2001	weak	
2002/2003	moderate	CP
2004/2005	moderate	CP
2006/2007	moderate	Mixed
2007/2008	moderate	
2009/2010	moderate	CP
2010/2011	moderate	

601

602 **Table 2: slope of the linear fit for oxygen, temperature, salinity, nitrate and nitrite as a function of depth over the period 1999-2011.**

603 The slope for thermocline and oxycline depths are also provided as a function of season. The confidence level estimated based on a  
 604 Student's T-test is indicated in parenthesis when larger than 80%.

605

Depth (meter)	O <sub>2</sub> (μmol kg <sup>-1</sup> decade <sup>-1</sup> )	T (°C decade <sup>-1</sup> )	S (PSU decade <sup>-1</sup> )	Nitrate (μmol L <sup>-1</sup> decade <sup>-1</sup> )	Nitrite (μmol L <sup>-1</sup> decade <sup>-1</sup> )
0	24.03 (90%)	-0.04	0.026	0.93	0.11
10	47.55 (95%)	0.53 (80%)	0.013	-0.17	-0.22 (80%)
25	40.35 (95%)	0.65 (90%)	0.025 (80%)	-1.67	-0.01
50	14.40 (85%)	0.50 (90%)	0.003	0.01	-0.15
75	6.04 (90%)	0.34 (90%)	-0.002	1.85	-0.57
90	6.76 (95%)	0.42 (95%)	-0.001	2.51 (80%)	-0.75
100	7.53 (95%)	0.46 (95%)	0.003	2.95 (80%)	-0.88
<b>Annual</b>	<b>OMZ (m decade<sup>-1</sup>)</b> -0.64 (95%)	<b>Thermocline (m decade<sup>-1</sup>)</b> -0.30 (95%)			
<b>Seasonal</b>	<b>Summer</b> -0.74 (95%)	<b>Winter</b> -0.77 (95%)	<b>Summer</b> -0.63 (95%)	<b>Winter</b> 0.03	
	<b>Fall</b> -0.76 (95%)	<b>Spring</b> -0.69 (95%)	<b>Fall</b> -0.49 (95%)	<b>Spring</b> -0.48 (95%)	

606

607

608

609

610

611

612

613

614

615



616

617

618 **Table 3: Correlation values between the PC time series, the ENSO indices (E, C) and Kelvin waves amplitude (EKW 1 and 2) for**  
 619 **the periods. Shading indicates the correlation values significant at the 95% level. E is the Eastern Pacific El Niño index) and C is the**  
 620 **Central Pacific index as defined by Takahashi et al. (2011). Note that the C index accounts for both Central Pacific El Niño events**  
 621 **and La Niña events.**

622

	<b>E</b>	<b>C</b>	<b>EKW1</b>	<b>EKW2</b>
<b>Period</b>	<b>1996-2010</b>			
<b>PC1</b>	0.72	0.31	0.38	0.61
<b>PC2</b>	0.28	-0.27	0.00	0.07
<b>Period</b>	<b>1999-2010</b>			
<b>PC1</b>	0.23	0.58	0.33	0.53
<b>PC2</b>	-0.10	0.09	0.08	-0.01

623

624

625 **Figures caption**

626 **Figure 1.** Location of the sampling station (St 4; 20 nm, 145 m depth) in the coastal upwelling ecosystem off central Peru, Callao (12° 02'  
627 S; 77° 29' W).

628 **Figure 2.** Time series of temperature (°C) (a), salinity (b) and dissolved oxygen ( $\mu\text{mol kg}^{-1}$ ) (c) during the 1996-2011 study years. Black  
629 dots indicate the location in space and time of the data and a DIVA 2017 graphic interpolation was used for the visualization of the data.

630 **Figure 3.** Temperature (top) and Oxygen (bottom) anomalies relative to the mean climatology (a, c) and the respective climatologies (b,d).  
631 The  $45 \mu\text{mol kg}^{-1}$  iso-contour for total oxygen concentration (oxycline) is overplotted in c) as a thick black line while the  $90 \mu\text{mol kg}^{-1}$  iso-  
632 contour for anomalies is drawn in thin black line in order to visualize the amplitude of the anomalies during the 1997/98 El Niño event. The  
633 number of years to derive the climatology is indicated in b) and d) below the calendar months.

634 **Figure 4.** Time series of nitrate (a), nitrite (b), silicate (c) and phosphate (d) during 1996-2011. Units are  $\mu\text{mol L}^{-1}$ . Black dots represent the  
635 data and the figure present a DIVA 2017 graphic interpolation only for the visualization of the data.

636 **Figure 5.** Time series of N deficit ( $\mu\text{mol L}^{-1}$ ) at St. 4 off Callao during 1996-2011. Black dots represent the data and the figure present a  
637 DIVA 2017 graphic interpolation only for the visualization of the data.

638 **Figure 6.** Projection of the data onto the (red line) E and (blue line) C indices for a) oxygen, b) temperature, c) salinity, d) nitrate and e)  
639 nitrite.

640 **Figure 7.** Percentage of variance explained by the projection of the data on the E and C modes as a function of depth for temperature (red),  
641 salinity (blue), oxygen (dark green), nitrate (purple) and nitrite (orange).

642 **Figure 8.** Evolution of the (a, b) amplitude of the Equatorial Kelvin Waves (EKW) anomalies at  $90^\circ\text{W}$  for the first (EKW\_1) and second  
643 (EKW\_2) baroclinic modes. Units are cm (equivalent sea level). The standard deviation is indicated by the horizontal dashed lines. Time  
644 resolution of the data is every 5 days, (c) depth of the thermocline; (d) OMZ upper boundary depth and (e) Fixed Nitrogen deficit (Ndef)  
645 at 50 m (f) at St. 4 off Callao during 1996-2011. On the right hand side of each timeseries, the global wavelet spectrum with significance level  
646 at 95% are shown (g-j). The 95% confidence level estimated from a red noise (Markov model).

647 **Figure 9.** Combined EOF analysis of temperature, salinity, oxygen, nitrate and nitrite for the periods (top) 1995-2010 and (bottom) 1999-  
648 2010. (a, d) PC timeseries and (b, c, e, f) mode patterns for the first two EOF modes. A 6-month low-pass filter was applied to the data and  
649 the data have been normalized prior to carrying the EOF analysis so that unit is adimensionalized.

650

651  
652  
653  
654  
655  
656  
657  
658  
659  
660  
661  
662  
663  
664  
665  
666  
667  
668  
669  
670  
671  
672

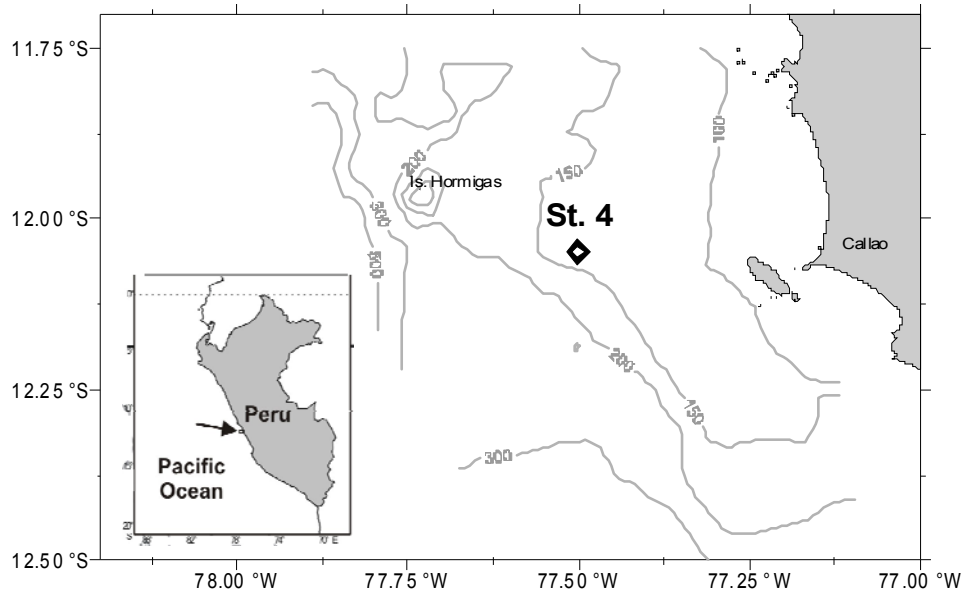
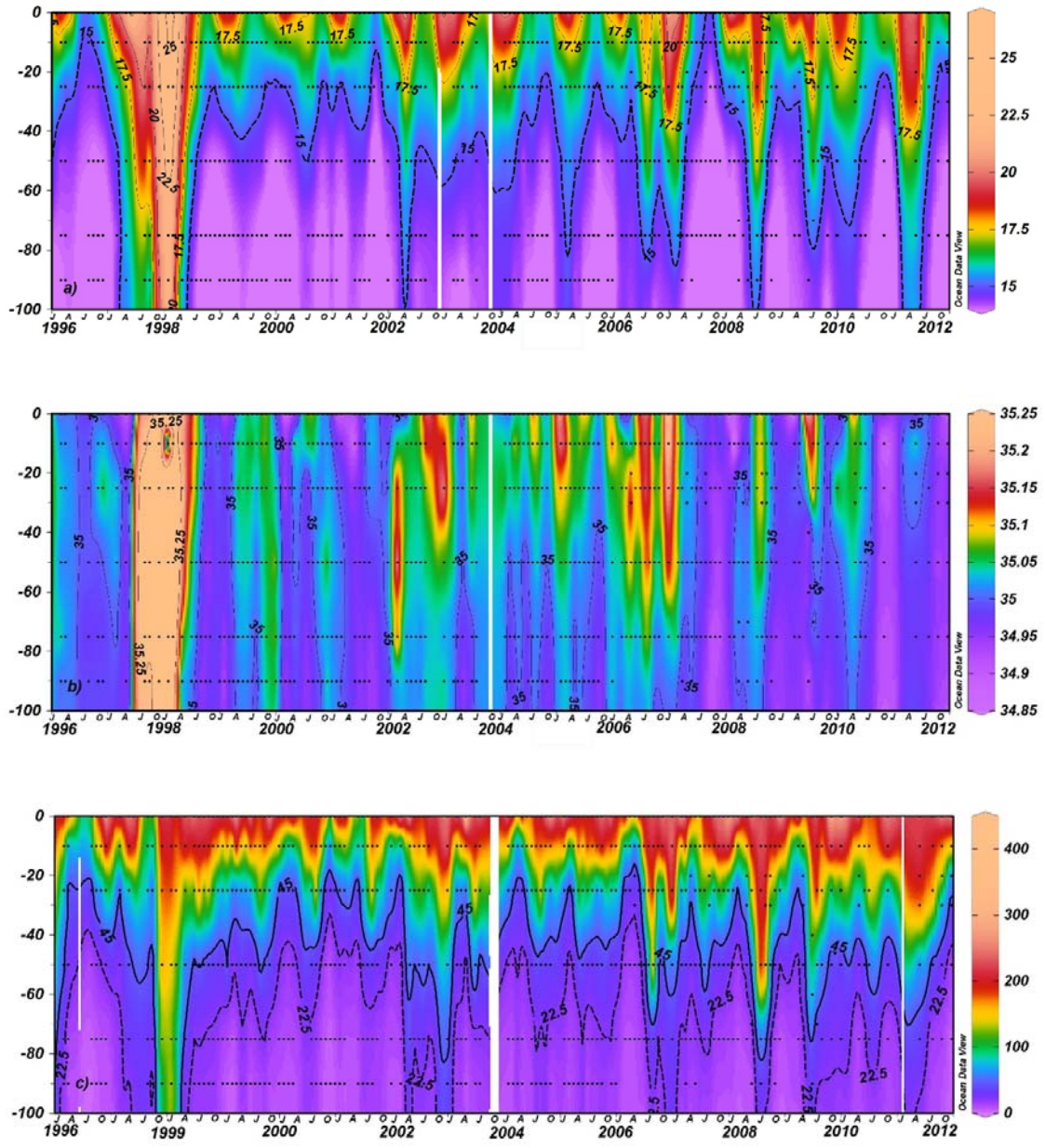


**Figure 1.**

673  
674  
675  
676



677 Figure 2.  
678  
679  
680  
681  
682  
683  
684  
685

686

687

688

689

690

691

692

693

694

695

696

697

698

699

700

701

702

703

704

705

706

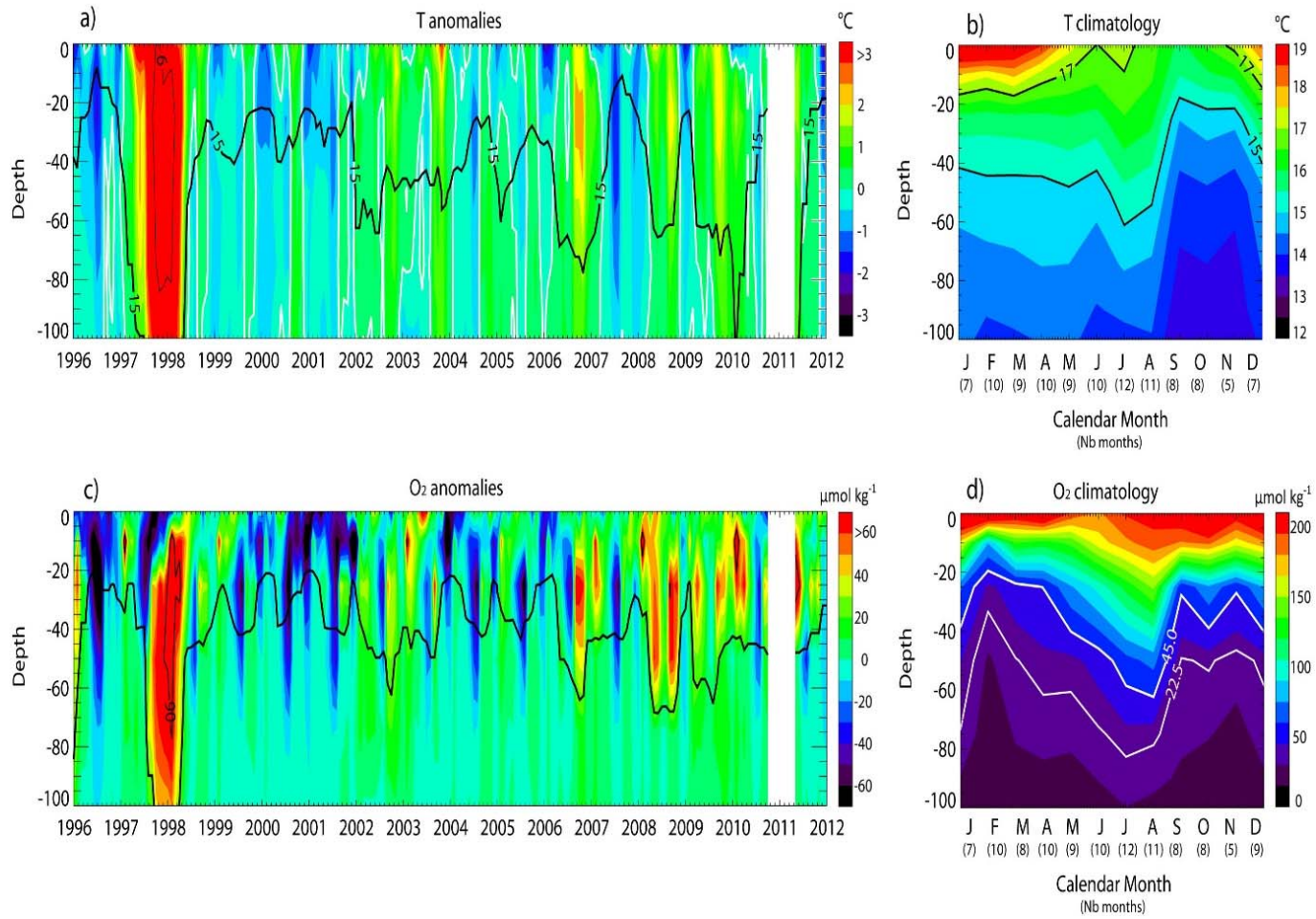
707

708

709

710

Figure 3.



711  
712  
713  
714  
715  
716  
717  
718  
719  
720  
721  
722  
723  
724  
725  
726  
727  
728  
729  
730  
731  
732  
733  
734  
735  
736  
737  
738  
739  
740  
741  
742  
743  
744  
745  
746  
747  
748  
749  
750  
751  
752  
753  
754  
755  
756  
757

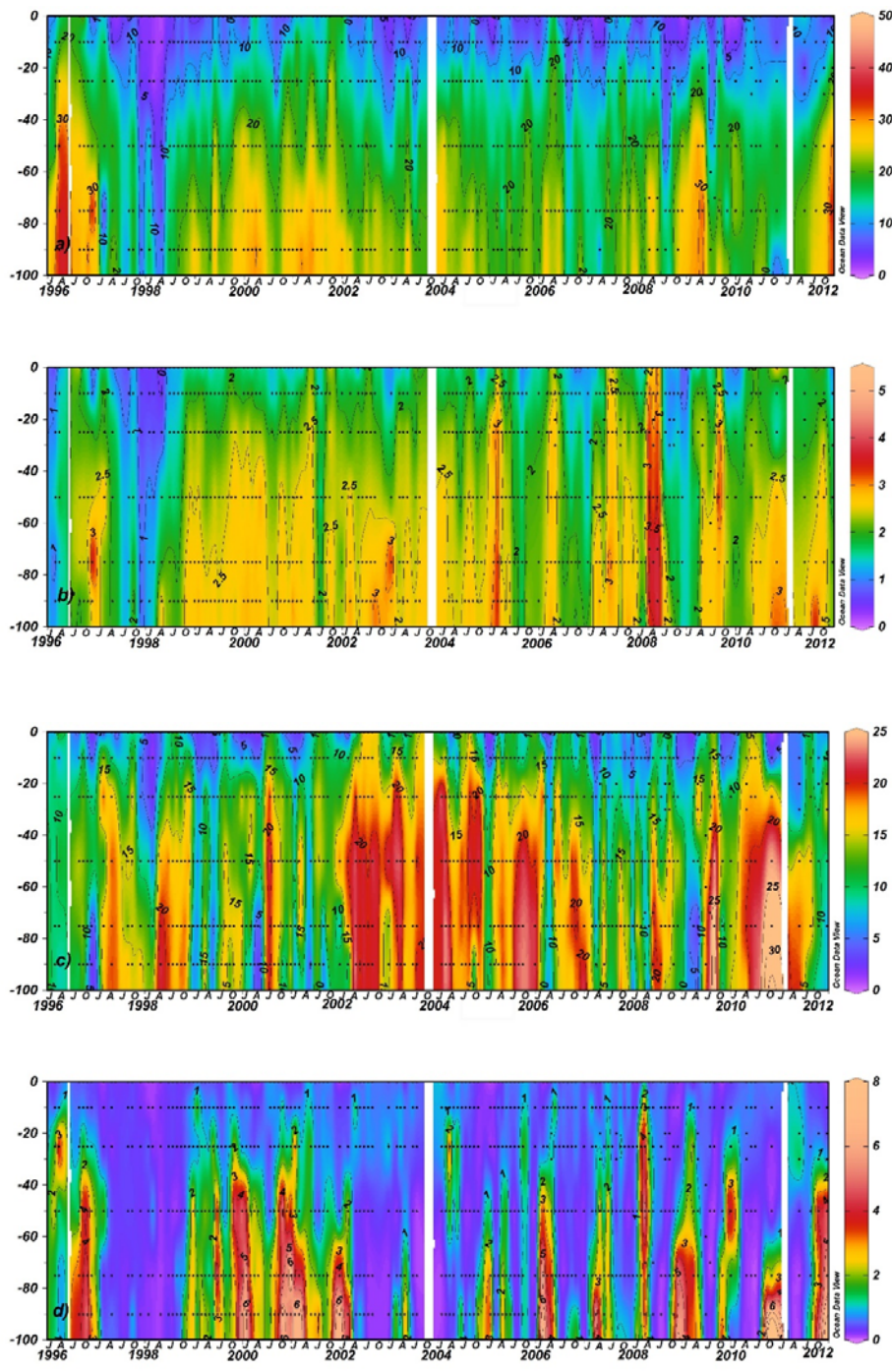
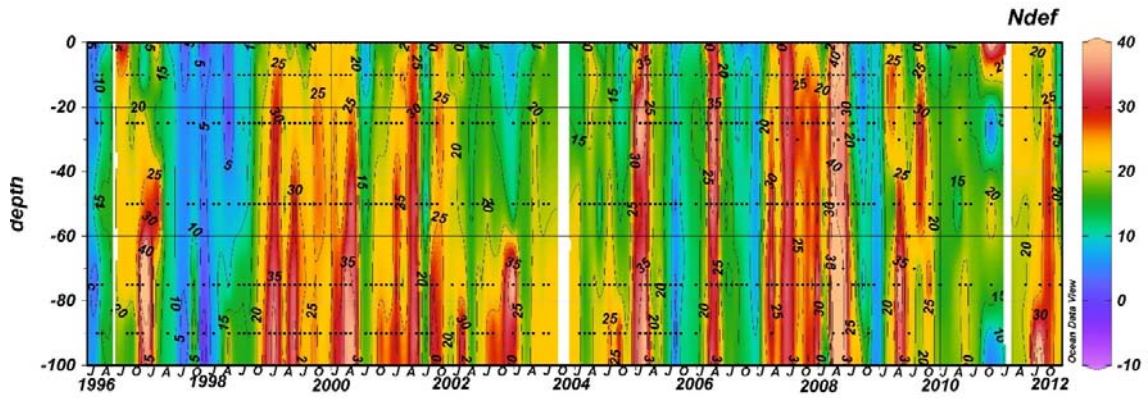


Figure 4.

758

759



760

761

762

763

764

765

766

767

768

769

770

771

772 **Figure 5.**

773

774

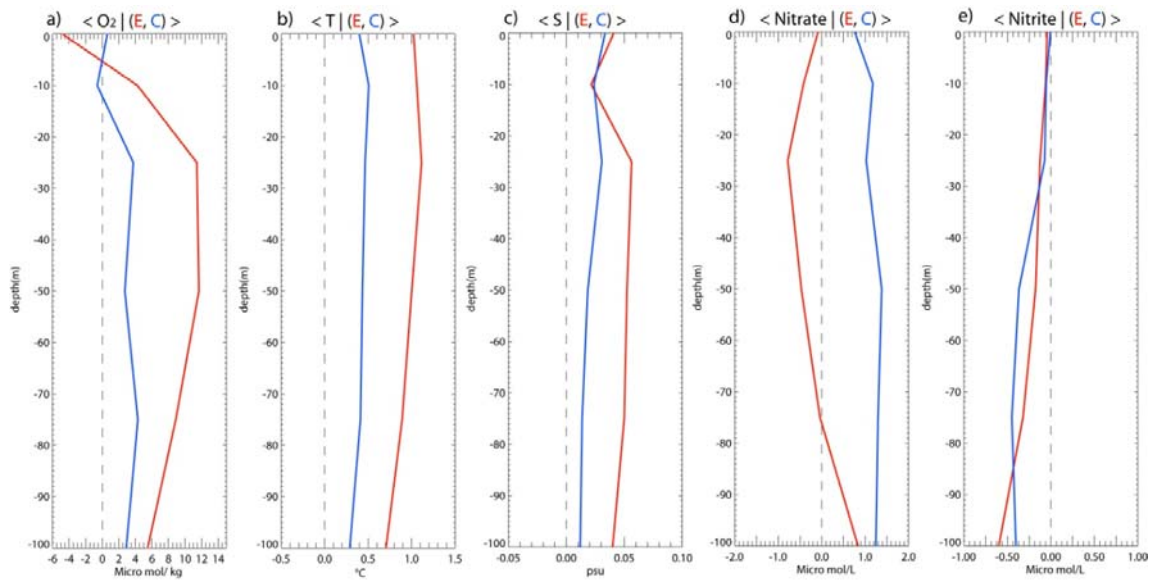
775

776

777

778

779



780

781

782

783

784

785

786 **Figure 6.**

787

788

789

790

791

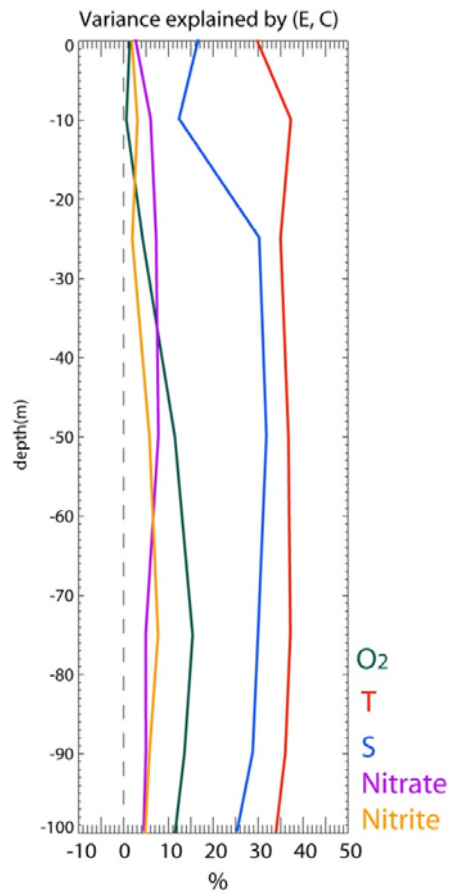
792



793

794

795



796

797 **Figure 7.**

798

799

800

801

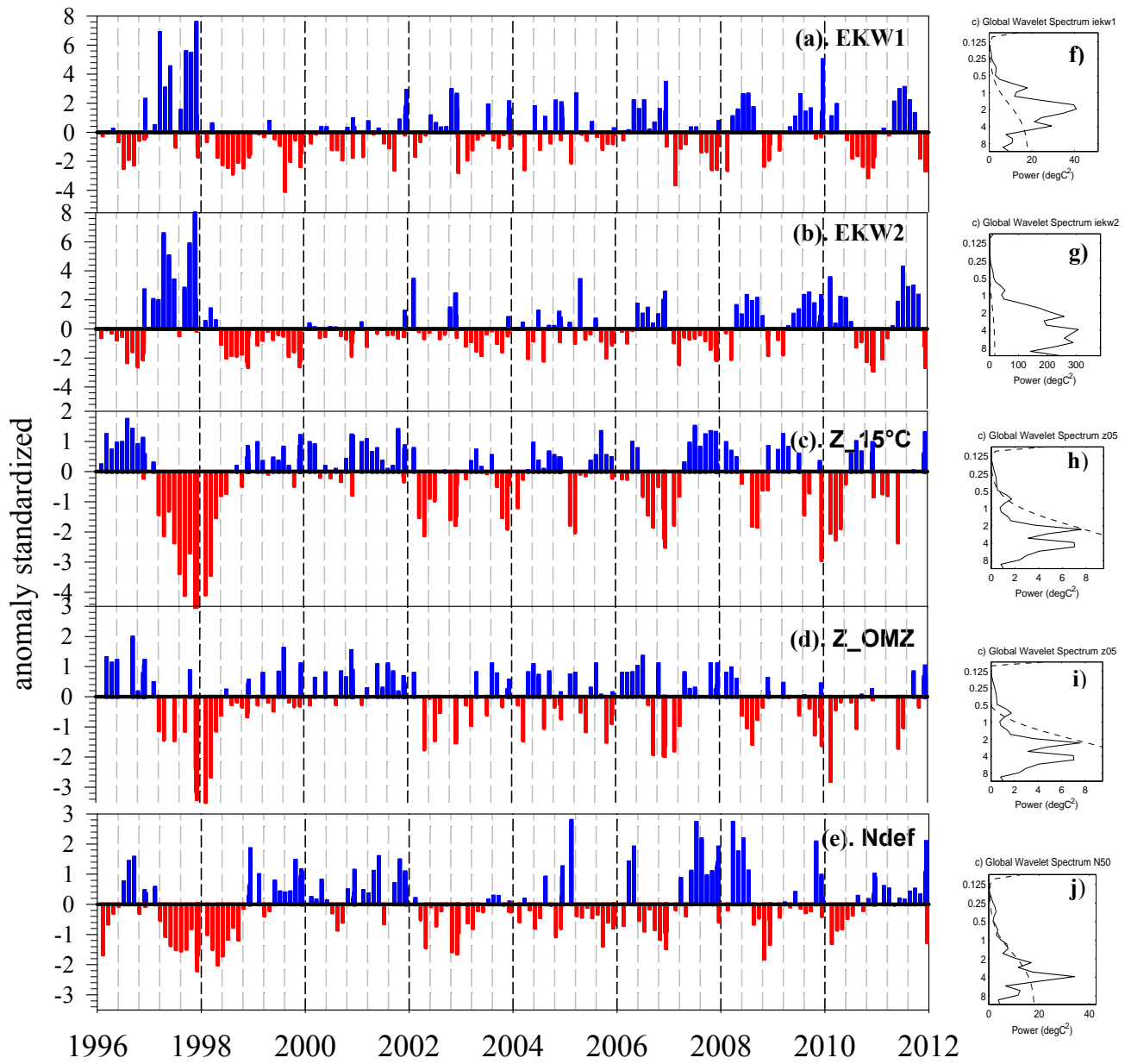
802

803

804

805

806



807

808

809

810 **Figure 8.**

811

812  
813  
814  
815  
816  
817  
818  
819  
820  
821  
822  
823  
824  
825  
826  
827  
828  
829  
830  
831  
832  
833

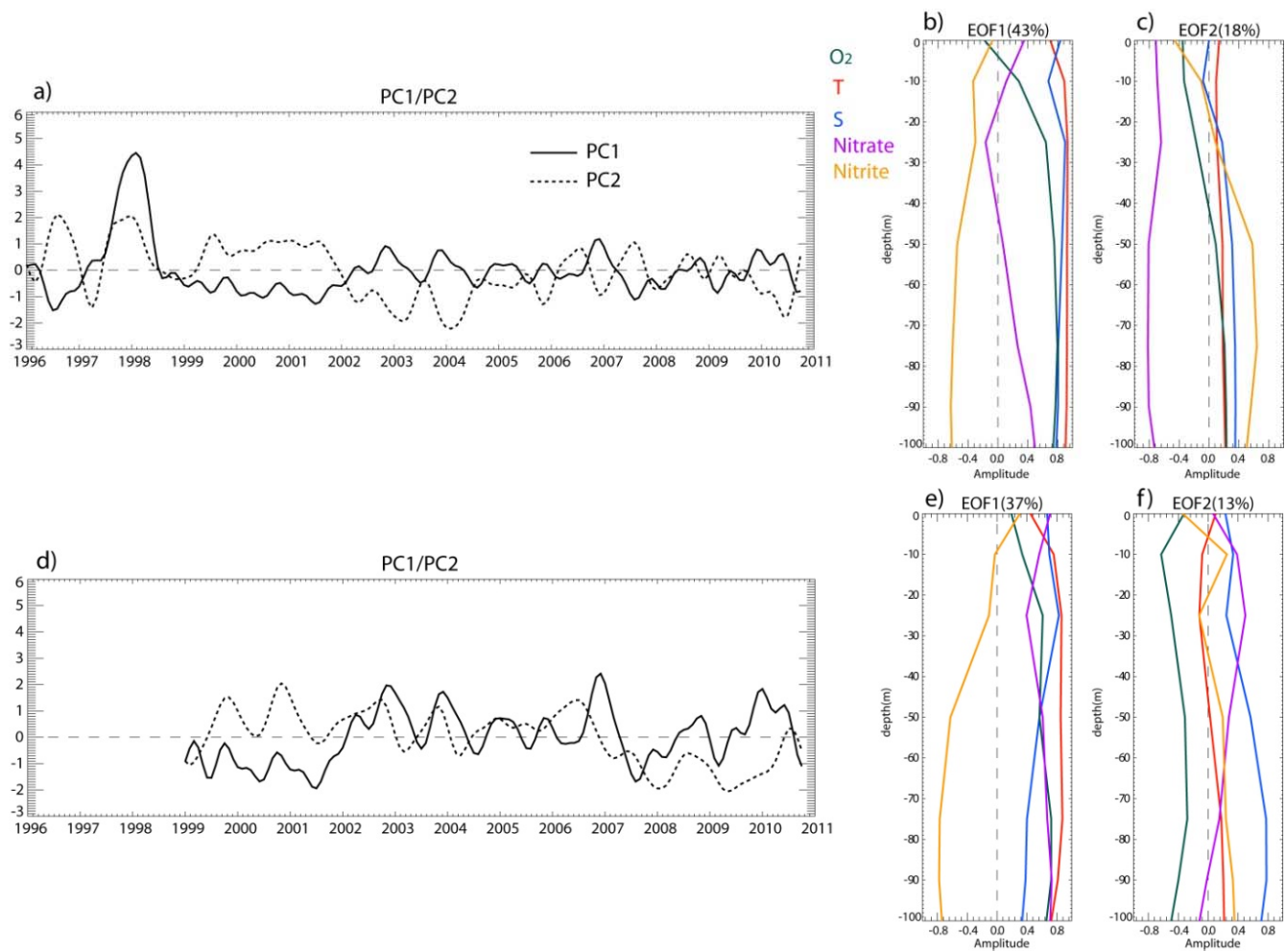


Figure 9.